https://doi.org/10.5194/egusphere-2024-106
Preprint. Discussion started: 31 January 2024

Exploring Accumulation Dynamics in the Pearl River Estuary from Lagrangian Perspective

Mingyu Li[1], Stocchino Alessandro[2,3], Zhongya Cai[1,3], Tingting Zu[4]

[1]State Key Laboratory of Internet of Thing for Smart City, Department of Ocean Science and Technology, University of Macau, Macau, 999078, China

[2]Department of Civil and Environmental Engineering, The Hong Kong Polytechnic University, Hong Kong, 999077, China

[3]Center for Ocean Research in Hong Kong and Macau (CORE), Hong Kong, 999077, China

[4]State Key Laboratory of Tropical Oceanography, South China Sea Institute of Oceanology, Chinese Academy of Sciences, Guangzhou, 510301, China

Correspondence to: Zhongya Cai (zycai@um.edu.mo); Tingting Zu (zutt@scsio.ac.cn)

Abstract. Utilizing Lagrangian methods and Markov Chains, we examined the water accumulation dynamics in the Pearl River Estuary (PRE), which are essential for understanding estuarine mass distribution and ecosystem management. Influenced by plume fronts and velocity convergence, we observed significant bottom-layer accumulations in the western estuary and Hong Kong waters during summer, while accumulation region shifts to upper estuary and Macau waters in winter. Generally, there is notable correlation between the horizontal velocity divergence ($\nabla_h\vec{V}_h$) and the accumulation probability, where local negative $\nabla_h\vec{V}_h$ fosters the accumulation. However, the net accumulation depends on the cumulative effects of convergence along the trajectories, not just its Eulerian pattern. The plume fronts also obstructed the particles transport and played an important role in the accumulation. Combined with trajectories, subregions with distinct accumulation patterns and interconnection among them were identified. During summer, western estuary and Macau waters with substantial net negative $\nabla_h\vec{V}_h$ and strong front were major accumulation targets, which attracted particles from the whole estuary. Conversely, the eastern estuary and Hong Kong waters exhibit significant westward motions, influencing the western side. In winter, particles were more likely to accumulate in their original regions. The upper estuary becomes a major accumulation area due to the obstructive density front, while Hong Kong waters show a tendency to diverge throughout the estuary. Sensitivity experiments illustrated that tides mainly promoted the accumulation in the western and upper estuary regions during winter and in Macau and HK waters during summer. Additionally, larger river discharges were conducive to the seaside transport in the upper and western estuary during summer and in the HK regions during winter.

https://doi.org/10.5194/egusphere-2024-106
Preprint. Discussion started: 31 January 2024

1 Introduction

Located in southern China and extending over the shelf of the Northern South China Sea (NSCS) (Figure 1), the Pearl River Estuary (PRE) sustained large populations, economy, and valuable ecosystems. The circulations in the PRE and adjacent shelf exhibited the complex interplay of processes including seasonal winds, river runoff, tidal forces, and topographic modulation. Numerous research has been conducted to understand the circulations dynamics in the PRE and its adjacent shelf regions (Ascione Kenov, Garcia, & Neves, 2012; Banas & Hickey, 2005; Gong, Shen, & Hong, 2009; C. He, Yin, Stocchino, & Wai, 2023; C. He, Yin, Stocchino, Wai, & Li, 2022; Liu, Zu, & Gan, 2020). Such as tidal currents, predominantly semi-diurnal and diurnal, played a crucial role in the estuary's stratification structures (Mao, Shi, Yin, Gan, & Qi, 2004). The seaward gravitational current controlled the upper estuary and northern part of the lower PRE, while southern part was further controlled by the geostrophic intrusive currents (Zu & Gan, 2015). Additionally, the wind driven shelf currents played an important role in the estuarine circulation of the lower part of the PRE (Dong, Su, Ah Wong, Cao, & Chen, 2004).

In recent decades, the estuary's health and sustainability have been increasingly imperiled by environmental issues caused by anthropogenic activities such as eutrophication (Dai et al., 2006; Fok & Cheung, 2015). The estuarine circulation and its associated mass transport were critical in addressing these environmental challenges. The specific areas of water accumulation and the extent of its exchange with the open sea significantly impacted the dispersion of oceanic pollutants and the biogeochemical health (Acha, Mianzan, Guerrero, Favero, & Bava, 2004; Hinojosa, Rivadeneira, & Thiel, 2011). In the estuaries, areas of accumulation were characterized by stronger horizontal convergence (Wang et al., 2022). Under the transport of the estuarine current, the total organic carbon was more likely to concentrate within specific sub-domains of the PRE (e.g., Macau, Shenzhen Bay and Hong Kong) (Guo, Ye, & Lian, 2016). Similarly, studies on hypoxia have shown that the convergence of buoyancy-driven currents and wind-driven shelf flows contributed to the formation of stable water columns, providing favorable conditions for the development of hypoxic zones (e.g., D. Li et al. (2021), X. Li et al. (2020)). However, due to the complex circulation dynamics, the mass accumulation processes remained largely unexplored.

The Lagrangian tracking method provided an effective way to analyze the transport processes in physical oceanography(Jalón-Rojas, Wang, & Fredj, 2019; van Sebille et al., 2018). It analyzed large sets of virtual particle trajectories calculated from the simulated Eulerian three-dimensional and time-varying velocity fields, which captured complex real-world dynamical processes. Their applications extended across various domains, including inter-ocean exchange(Haza, Özgökmen, & Hogan, 2016), pathways analysis (Jalón-Rojas et al., 2019), and the impact of ocean currents on ecosystem (Chenillat et al., 2015; Dawson, Sen Gupta, & England, 2005; Lebreton, Greer, & Borrero, 2012; Paris et al.,

https://doi.org/10.5194/egusphere-2024-106
Preprint. Discussion started: 31 January 2024

2012).

In this study, the Lagrangian tracking and analysis were utilized to examine the features of the accumulation regions in the estuary-shelf system of PRE, and explored the role of different forcing factors. The results were helpful to deepen the understanding of the environmental effects of the multi-scale processes. The paper was organized as follows: Sect. 2 presented the Lagrangian model and numerical solutions of Markov Chain. The findings on accumulation region and transport connections in the PRE were discussed in Sect. 3. And finally, Sect. 4 provided the conclusions of the study.

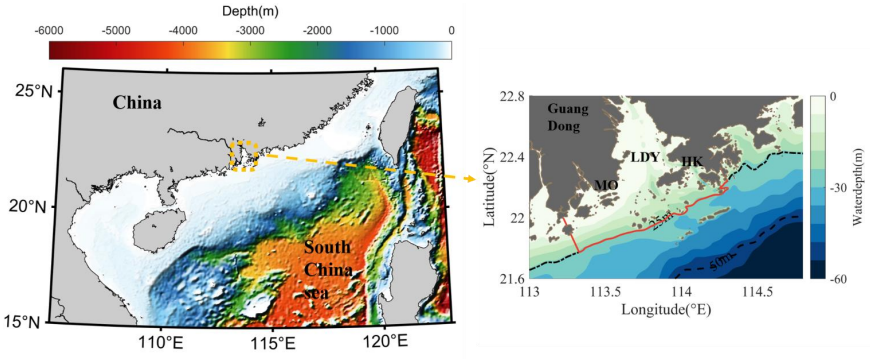

Figure 1: Location and topography of the Pearl River Estuary and adjacent shelf. The black dotted and dashed lines represented the isobath of 25 m and 50 m. The red line defined the seaside boundary of the PRE. LDY, MO and HK represented Lingdingyang, Macau and Hong Kong, respectively.

2 Methods

2.1 Lagrangian particle tracking

In this study, the multiscale circulation in the PRE and adjacent shelf regions was simulated by implementing the Regional Ocean Modeling System (Shchepetkin & McWilliams, 2005). The model used an orthogonal curvilinear grid, and the resolution gradually increased from ~ 1km over the shelf to ~ 0.1 km over the estuary and inner shelf. It had 30 vertical levels on terrain-following s-coordinates (Song & Haidvogel, 1994), with higher resolutions (0.2 m) in the surface and bottom boundary layers.

Considering the complex local hydrodynamics, we adopted the seasonal forcing to simulate the climate conditions in the PRE, which fully represented the motion condition in the real world. Data of shelf currents were obtained by the coarser-resolution simulation. The statistics of atmosphere forcing and monthly averaged river discharge rate were calculated by the European Center for Medium Weather Forecasting (ECMWF). Tidal current simulations considering the forcing along

https://doi.org/10.5194/egusphere-2024-106
Preprint. Discussion started: 31 January 2024

the open boundaries were obtained from Zu, Gan, and Erofeeva (2008), which including the tidal harmonic constants (M2, S2, K2, N2, K1, O1, P1, Q1 as well as the M4). The simulation was validated using the long-term remote sensing and local observations and was used in the studies of PRE (Cai, Liu, Liu, & Gan, 2022; Chu et al., 2022; Cui, Cai, & Liu, 2023).

Using the Eulerian flow fields and turbulent mixing from the hydrodynamic model, particles trajectories were traced by a three-dimensional off-line Lagrangian TRANSport model (LTRANS v.2b) (Chu et al., 2022; Liang et al., 2021; Elizabeth WEW North et al., 2011). The tracking model included several dynamical processes such as turbulent mixing, particles behavior and other complicated hydrodynamic processes. The results of the computations reasonably described the Lagrangian dynamics within different layers in the estuary-shelf system. The 4th order Runge-Kutta scheme was implemented to handle the advective terms and further yield accurate particle trajectories (Dippner, 2009). Considering the random walk of water parcels in the ocean, the model adopted different diffusivity coefficient to control the vertical and horizontal turbulence, respectively (E. W. North, Hood, Chao, & Sanford, 2006; Zhong & Li, 2006).

In our numerical experiments, the particles were releasing for 30 days in January and July to represent the typical winter and summer respectively. Each day, 8386 particles were released uniformly covering the whole PRE and tracked for 30 days after releasing.

2.2 Markov Chain

In this study, to investigate the accumulation features and connectivity among different parts of the domain, we implemented the Markov Chains statistical analysis to describe the future state of a random variable, which was based on the particle original state positions to compute a proper transition matrix (K. L. Drouin & Lozier, 2019; Kimberley L. Drouin, Lozier, Beron-Vera, Miron, & Olascoaga, 2022; Miron, Beron-Vera, Helfmann, & Koltai, 2021; Miron et al., 2019; Miron et al., 2017; van Sebille et al., 2018). To this end, we subdivided the study area into rectangular grids with dimensions of 0.1 degree, then the probability of particles moving between different grids within the time interval of dt could be calculated as:

$$p^t = \frac{n_{ij}^{t+dt}}{n_i^t}, \quad (1)$$

where $n_{i,t0}$ represented number of particles released in grid i at initial time t. n_{ij}^{t+dt} represented number of particles arrived at grid j from grid i after interval time dt. Thus, $p^{n_{ij}^{t+dt}}$ varied for different releasing grid i, arriving grid j and the time period $(t,\ t+dt)$. Then the evolution of the initial distribution (D^t) into a future state (D^{t+dt}) was achieved by the vector-matrix multiplication:

https://doi.org/10.5194/egusphere-2024-106
Preprint. Discussion started: 31 January 2024

$$D^{t+dt} = D^t \times p^t ,$$

(2)

In this study, the D^{t_0} was defined as a uniform initial distribution in the whole domain that $D^{t_0} = [1, 1, 1, \cdots 1]$. The D^{t_0+ndt} represented how the initial condition finally evolves under the complicated hydrodynamic motions. The high values in D represented the regions where the particles were more likely to accumulate. The transport matrix by Markov Chains helped to predict a longer timescale transport pathways and was widely used to explore the transport pathways and connectivity of water parcels between different regions, such as van Sebille et al. (2018) investigated the pathways of major current in the Agulhas Current, Kimberley L. Drouin et al. (2022) found that Caribbean and Gulf of Mexico didn't involve the water transition between North Brazil Current and 26°N effectively. According to the studies of Jönsson and Watson (2016) and Kimberley L. Drouin et al. (2022), the choice of dt did not significantly influence the results of transport pattern. For the present analysis we selected a value of the time interval (dt) of 2 days.

3 Results and Discussion

3.1 Transport accumulation and connectivity

Before checking the detailed transport structure, we first examined the offshore transport speed of particles after being released. Using all the particle's trajectories, Figure 2 showed the percentage of the particle remaining inside the PRE during summer and winter, respectively. Here the seaside boundary of the PRE was defined by 25 m isobath (red line in Figure 1). Overall, the decaying speed was faster in summer than that in winter, with significant differences observed between the surface layer and bottom layer. Using a value of 20% as a threshold (green dotted line in Fig. 2), during summer, it showed about 80% of surface particles exited the estuary in approximately 10 days, while bottom particles took around 15 days. On the contrary, during the winter season with the reduced river discharges, the exit time was lengthened up to 20 days (for the surface particles) and 25 days (for the bottom particles). Thus, for the whole domain, after being tracked for 30 days, the majority of the particles left the estuary region, and the particle trajectories were used in the following analysis. Using the trajectories of the released particles within 30 days, we explored the final evolved state, which quantified the probability that the particles would accumulate in different regions as the result of the complex hydrodynamics of the estuarine circulation.

https://doi.org/10.5194/egusphere-2024-106
Preprint. Discussion started: 31 January 2024

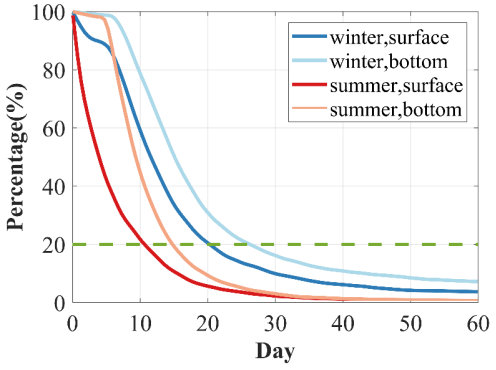

Figure 2: The changes of particle percentage remaining in the estuary during tracking.

During summer, associated with the intensified river discharge and offshore transport, the surface particles tended to quickly exit outside the estuary. This resulted in a very low accumulation probability (Fig. 3a). On the contrary, in the bottom layer (Fig. 3b), the current flowed northwestward inside the estuary because of gravity circulation. Besides, driven by the southwesterly monsoon, coastal upwelling was formed over the NSCS shelf with intensified bottom onshore intrusion from shelf. Consequently, the high values of accumulation probability were observed for the bottom layer especially in the western side, southwestern sides (near Macau) and Hong Kong waters (Fig. 3b). Although those regions were close to the open shelf, they were more likely to be the primary accumulation zones that capture particles initially released in other areas of the domain. Cruise observation data (during 2014-2018) also showed that those regions generally have high frequency of hypoxia occurrence under the accumulation effect from hydrodynamic processes (D. Li et al., 2021). During winter (Fig. 3c-d), when weaker discharges occurred, the gravitational circulation was generally preserved, but with weakened intensity. The bottom waters invaded further landward in the estuary, while the seaward flow was still observed in the surface layers. Over the shelf, because of the extensive northeasterly wind, the shelf current flowed southwestward and features with bottom offshore transport. Associated with the changes of the circulation, the accumulation probability in the upper layer increased but still with a much smaller magnitude than the one at the bottom. At the bottom, the accumulation regions moved shoreward, especially in the upper estuary and western estuary.

https://doi.org/10.5194/egusphere-2024-106
Preprint. Discussion started: 31 January 2024

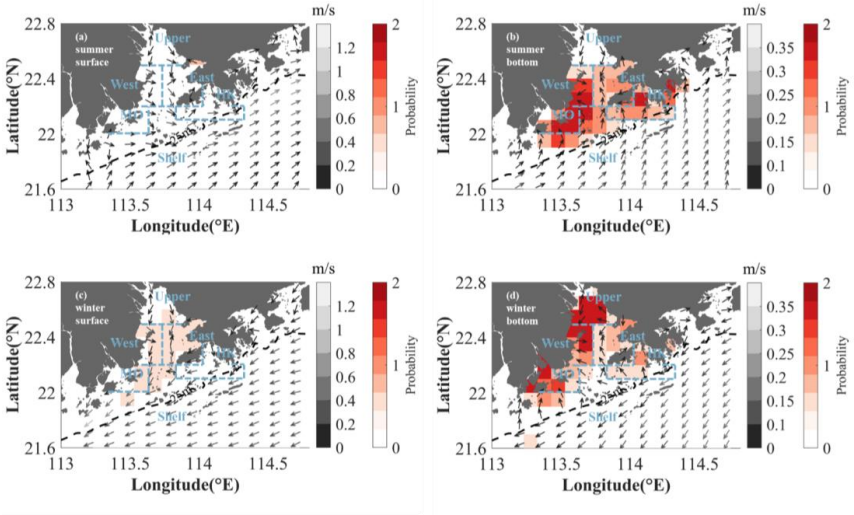

155 **Figure 3: (a–b) Accumulation probability (color, D in Eq. (2)) and mean velocity (arrows) at the surface and at the bottom during summer. The gray colorbar and red colorbar indicated the magnitude of the velocity and accumulation probability, respectively (c-d) were same as (a-b) but during winter.**

Based on the bottom accumulation probability distribution, we proposed to subdivide the study area into six subregions, 160 namely: Upper Estuary (UPPER), Western Estuary (WEST), Eastern Estuary (EAST), Hong Kong Water (HK), Macau Water (MO) and Shelf Water (SHELF). Then using the trajectories of the particles, we checked the probability of particles moving among each region during the tracking period (Fig. 4). The sensitivity experiments showed that the different tracking period would not significantly change the major pattern of the transport matrix. During summer (Fig. 4a), the original region always made a large contribution to the accumulations. For the WEST and MO regions, where had the 165 largest accumulation probability, the water accumulated there came from almost all the subregions including the shelf. The onshore intrusion from the shelf water and offshore motions from the upper estuary due to the river discharge converged the water there, as well as westward transport from EAST and HK, facilitated particle accumulation in WEST and MO. On the contrary, the EAST and HK regions accumulated particles mainly from the eastern side of the estuary. Despite the Eulerian currents suggested onshore intrusion from shelf and offshore transported from upper estuary toward these areas. 170 During the wintertime, the accumulation region moved shoreward that mainly occurred in the UPPER, WEST and MO regions (Fig. 4b), and the particles accumulated in those regions were mainly from the original releasing regions, thus the water there were more difficult to leave the original regions. It was also noticed that the HK water could affect almost the whole estuary, particularly contributing to accumulation in the WEST region.

https://doi.org/10.5194/egusphere-2024-106
Preprint. Discussion started: 31 January 2024

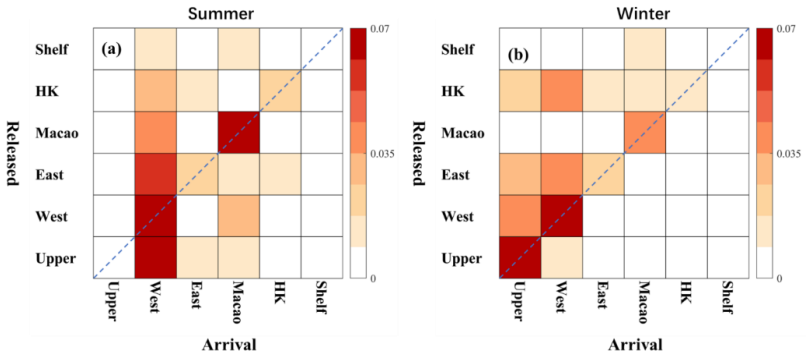

Figure 4: The connection between six subregions during the summer (a) and winter (b). The horizontal and vertical axes represented the arrival and releasing regions, respectively.

3.2 Hydrodynamic Control on the Accumulation

The divergence of the horizontal current, i.e., $\nabla_h \vec{V}_h = \frac{\partial u}{\partial x} + \frac{\partial v}{\partial y}$, where u and v represented the zonal and meridional velocity, was calculated to examine its influence on the identified bottom accumulation regions (Fig. 5a-b). Across the various identified subregions, a substantial negative correlation between the $\nabla_h \vec{V}_h$ and the accumulation probability was observed. There was a correlation coefficient of 0.87 in summer and 0.76 in winter, respectively. It suggested that the net negative $\nabla_h \vec{V}_h$, i.e. the convergence of the water, provided the favorable condition for the accumulation of water and particles. Such patterns were noted in the major accumulation regions, such as the WEST, MO and UPPER regions during both summer and winter time.

While it was also noted that for the EAST and HK regions, where showed the accumulation of particles, exhibited a weak net positive value of $\nabla_h \vec{V}_h$. This implied that the $\nabla_h \vec{V}_h$ facilitated accumulation under certain conditions, but the actual net accumulation should consider the cumulative effects of velocity convergence along the trajectories, which stayed at different locations during the movement. Spatial distribution of $\nabla_h \vec{V}_h$ also illustrated that the intensified negative values occurred in the region of the high accumulation probability (Fig. 5c-d), such as the substantial negative $\nabla_h \vec{V}_h$ observed in MO and WEST regions during summer, and in UPPRE region and central part of the HK region during winter. However, the Eulerian perspective of $\nabla_h \vec{V}_h$ presented a complex distribution of alternative positive and negative values. It did not lead to a straightforward identification of net accumulation areas. Instead, Lagrangian tracking offered a clearer understanding of these regions, as it captured the cumulative effects of water motion over time.

https://doi.org/10.5194/egusphere-2024-106
Preprint. Discussion started: 31 January 2024

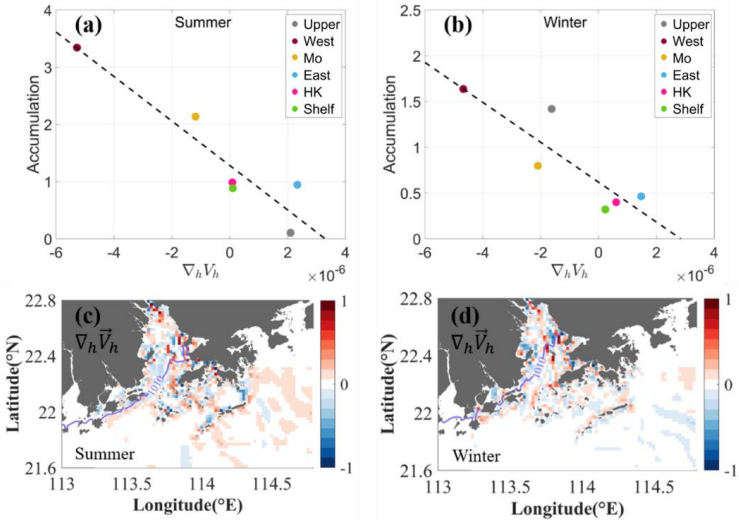

Figure 5: (a-b) Scatter plot of accumulation probability against $\nabla_h \vec{V}_h$ for various subregions during summer and winter, respectively. (c-d) Horizontal distribution of $\nabla_h \vec{V}_h$ during summer and winter. The $\nabla_h \vec{V}_h$ was normalized by the largest divergence value in this area. Purple lines represented the isopycnic line of 1010 kg·m^{-3}.

As a salt wedge estuary, the existing of salinity front would obstruct the particles transport and played an important role in the accumulation regions (Defontaine et al., 2020; Q. He et al., 2018; Vermeiren, Muñoz, & Ikejima, 2016). The coupling effect of velocity convergence and front made PRE accumulating particles in middle estuary and lower estuary during winter and summer, respectively (Malli, Corella-Puertas, Hajjar, & Boulay, 2022). During the summer, the heightened river discharge created the density front ($G = \sqrt{(\frac{\partial \rho}{\partial x})^2 + (\frac{\partial \rho}{\partial y})^2}$) (Fig. 6a), which affected the particles transport and promoted their accumulation. The location of the front, roughly aligned with the outer boundary region of profound negative $\nabla_h \vec{V}_h$ over the WEST and MO region (Fig. 5c), which further supported the accumulation in these regions as the front hinders their offshore movement. During winter, the intrusion reached the middle estuary, causing a blockage effect for the mass that tend to remain confined in the upper part of the estuary (Lima, Barletta, & Costa, 2015; Lima, Costa, & Barletta, 2014). This retention was likely to contribute to the observed accumulation patterns where particles remained in confined upstream due to the blockage effect of the front. The $\nabla_h \vec{V}_h$ in winter also reflected this dynamic that the region of negative values moved shoreward.

https://doi.org/10.5194/egusphere-2024-106
Preprint. Discussion started: 31 January 2024

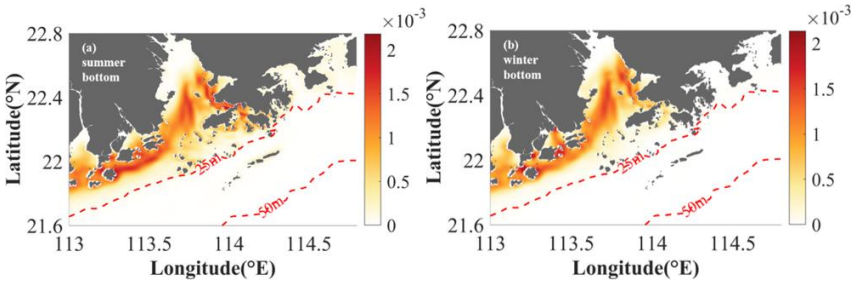

Figure 6: (a-b) The bottom front of density (kg·m^{-3}) in summer and winter.

3.3 Role of Tide and River

Since the tide and river were important factors affecting the estuarine circulations and associated mass transport in the PRE, two additional experiments were conducted to examine their contribution to the mass transport and accumulation. In the tide testing case, the tidal current was removed from hydrodynamic simulation; in the river testing case, discharge was reduced to 20% of standard cases. Using the same Lagrangian tracking and analysis approach, the accumulation regions and connection among different regions were investigated in the same way.

3.3.1 Tide

The influence of tide during summer mainly affected WEST, MO and EAST regions. The removal of tidal forces intensified particle accumulation in the WEST and northeastern parts of the EAST regions. Conversely, in the MO and HK regions, the absence of tides generally decreased the likelihood of accumulation, particularly in MO waters (Fig. 7a). In winter, when river discharge is weaker, tidal effects became crucial in accelerating offshore motion in the UPPER and EAST regions (Fig. 7b). In contrast, in the WEST regions, tides significantly obstructed particles from exiting the estuary, leading to a negative anomaly in accumulation when tides are removed.

Same as the standard case, there was the negative correlation between the $\nabla_h \vec{V}_h$ and the water accumulation (Fig. 7c-d). The decrease/increase of the summer accumulation probability in the MO/EAST region was associated with the weakening/strengthening of the net convergence of current due to the removal of tidal current. Similarly, the changes of the winter accumulation in the UPPER, WEST and EAST regions were related to the current divergence as well. However, it was also noted that the WEST and MO regions where had relatively strong $\nabla_h \vec{V}_h$, the changes in accumulation were not significantly influenced by this divergence.

The impact of tides on water transport among various identified subregions was investigated, as depicted in Fig. 7e-f. In

https://doi.org/10.5194/egusphere-2024-106
Preprint. Discussion started: 31 January 2024

summer, removing the tide resulted in a strengthened accumulation in the EAST and UPPER regions. The WEST regions continued to exhibit a strong converging trend, accumulating particles from across the estuary. Notably, in the absence of tides, the MO region no longer converged particles from other regions. Furthermore, particles originating from the EAST and UPPER regions ceased to reach the HK and MO regions. While during winter, the UPPER region displayed a heightened attraction to particles from the WEST, EAST, and MO regions. The converging trend in the WEST regions diminished rapidly, reducing its role as a significant trap for water from other regions. No significant changes in the EAST and HK, only for MO, it trapped more water from its own regions.

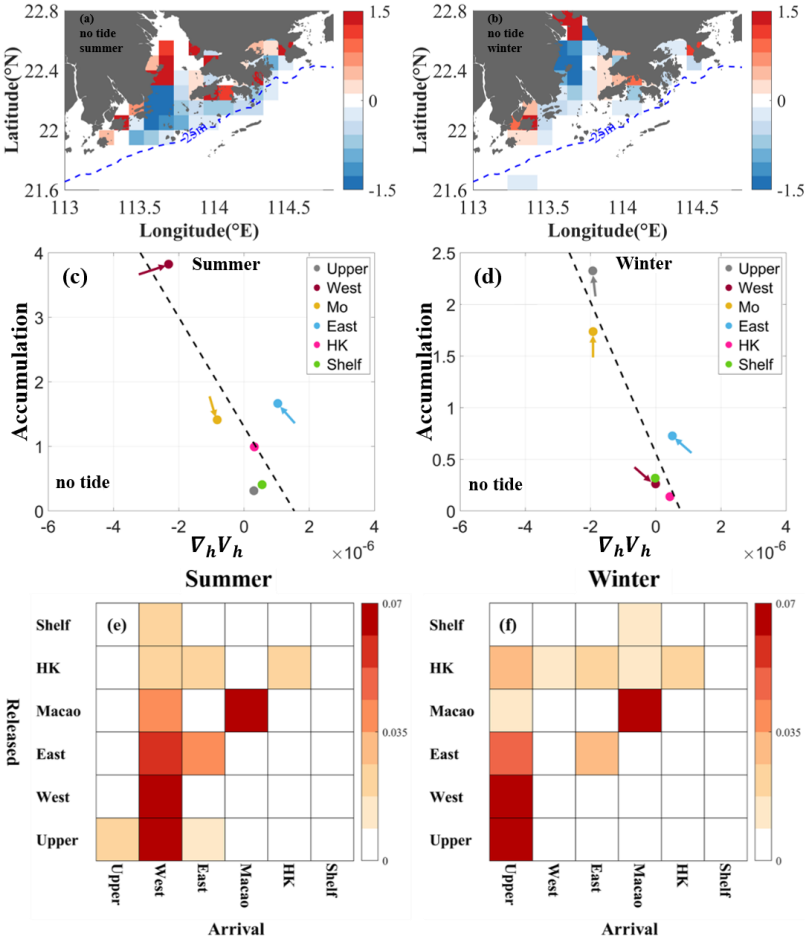

Figure 7: (a-b) Probability anomaly in the removing tide current case during summer and winter, respectively. (c-d) Scatter plot of accumulation probability against $\nabla_h \vec{V}_h$ for various subregions during summer and winter in removing tide case. The arrow represents the normalized changes of $\nabla_h \vec{V}_h$ and accumulation due to the removing of tide in each subregion. (e-f) The connection between six regions for the case without tides

https://doi.org/10.5194/egusphere-2024-106
Preprint. Discussion started: 31 January 2024

3.3.2 River discharge

The river discharge led to the opposite influence on the accumulation probabilities during summer and winter time, particularly in the UPPER and WEST regions. During the summer, the reduction of river discharge would largely converge particles in the UPPER and northern part of WEST regions. Over the southern part of WEST region, it caused the divergency of particles (Fig. 8a). By contrast, during winter, the river mainly converged the particles in UPPER and WEST regions that the strong negative anomaly formed in two regions with reduced river discharge (Fig. 8b). For the EAST region, the reduced river discharge tended to attract the particles to converge there and adjacent shelf. Generally, major changes in accumulation were governed by the current's convergency. In both seasons, variations in net velocity convergence resulted in corresponding changes in particle accumulation in the UPPER, WEST, and EAST regions (Fig. 8c-d).

In a same way, Figure 8e-f showed that with reduced river discharge, the transport connections in the UPPER, WEST and MO regions were greatly affected. For the UPPER regions, the converging ability became stronger, more particles from UPPER were remaining at origin region and no longer moved to EAST and MO regions. Furthermore, the reduced river discharge resulted in fewer particles from the MO regions accumulated in the WEST regions. Instead, the EAST regions contributed more to the accumulation in the WEST regions. During wintertime, interconnections among the six subregions remain similar to the standard case (Fig. 8f). It was also noted that the WEST regions converged less particles from the EAST and HK regions. And the MO regions attracted particles from the WEST regions instead of from Shelf.

https://doi.org/10.5194/egusphere-2024-106
Preprint. Discussion started: 31 January 2024

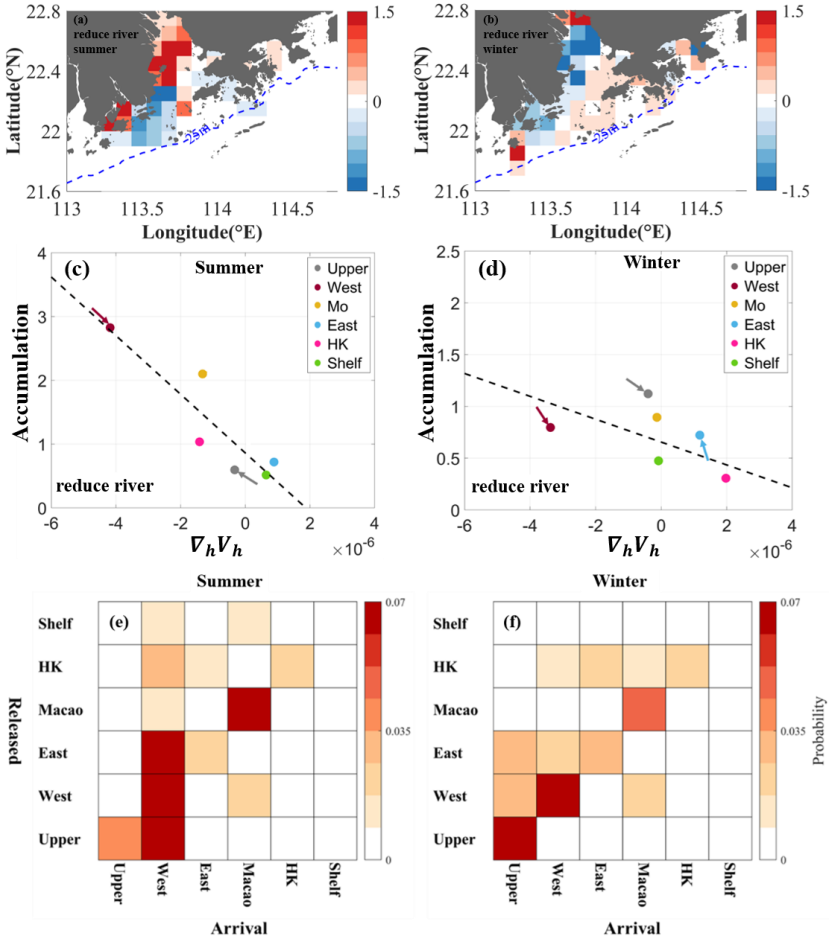

Figure 8: (a-b) Probability anomaly in the river reduced case during summer and winter, respectively. (c-d) Scatter plot of accumulation probability against $\nabla_h \vec{V}_h$ for various subregions during summer and winter in river reduced case. The arrow represents the normalized changes of $\nabla_h \vec{V}_h$ and accumulation due to the reduction of discharge in each subregion. (e-f) The connection between six regions for the case with reduced river discharge.

4 Conclusions

Understanding the accumulation dynamics in the PRE was crucial to explore the mass distributions in the estuary and environment protection. In this study, the Lagrangian method and Markov Chains were applied to illustrate the accumulation trend across different PRE regions in typical monsoon seasons.

The tracking results illustrated that the decaying speed of the particles in the estuary was faster in summer than that in winter, with significant differences observed between the surface layer and bottom layer. Generally, 80% of particles will

https://doi.org/10.5194/egusphere-2024-106
Preprint. Discussion started: 31 January 2024

leave the estuary by 15 days and 25days, respectively in summer and winter. Based on the trajectories of the released particles within 30 days, the probability that the particles would accumulate in different regions as the result of the complex hydrodynamics of the estuarine circulation were examined in detail.

The accumulation probabilities on the surface were quite small due to the strong wind stress and river discharge. But for bottom cases, high accumulations were observed in the western side of estuary near the shelf and Hong Kong waters during summer, while changed into along upper estuary and Macau during winter (Fig. 9). These accumulation zones exhibited shoreward movement in winter and seaward movement in summer at bottom layer. According to the accumulation patterns, we identified six subregions in the PRE: UPPER, WEST, EAST, MO, HK and SHELF. Across the subregions, there was a substantial correlation between the $\nabla_h \vec{V}_h$ and the accumulation probability, the negative $\nabla_h \vec{V}_h$ provided the favorable condition for the accumulation of water and particles. However, it was also noted that the actual net accumulation should consider the cumulative effects of velocity convergence along the trajectories. The Eulerian pattern of $\nabla_h \vec{V}_h$ could not lead to a straightforward identification of net accumulation areas. As a salt wedge estuary, the existence of salinity fronts also obstructed the particles transport and played an important role in the accumulation regions.

Combined with the bottom particle pathways, the accumulation connections between six subregions were illustrated. During summer, WEST and MO with substantial net negative divergence and strong front were powerful accumulation targets, which attracted particles from almost the whole estuary. EAST and HK waters showed westward motions, particles from here could arrived at western estuary. In winter, the accumulation regions showed self-correlations, particles were more likely to remain in original regions. UPPER became major accumulation regions due to the block of the density front. HK waters diverged into whole estuary, particularly contributed to accumulation in the WEST regions.

The sensitivity experiments were conducted to evaluate the effects of tidal forcing and river discharge on the accumulation patterns. Tides mainly promoted the accumulation in the WEST and UPPER regions during winter and in the MO and HK regions during summer (Fig. 9). And larger river discharges were conducive to the seaside transport in the UPPER and WEST during summer and in the HK regions during winter. What's more, tidal currents took an obvious influence for UPPER in winter, which could converge more particles from lower estuary. And the attractions of WEST became weakened when removing the tide. During summer, removing tide was helpful for converging particles in the EAST. For MO waters, it only traps particles released by itself. Less river discharge showed different influence on the accumulation regions. When reduced the river discharge in winter, the seaside transport was obstructed, for particles from UPPER would not arrive at the EAST and MO regions, and converged MO waters into the WEST regions. While in summer, the accumulation probability in released regions increased, the westward transport of HK and EAST waters became weakened. The intrusion from SHELF waters into MO regions was also decreased.

https://doi.org/10.5194/egusphere-2024-106
Preprint. Discussion started: 31 January 2024

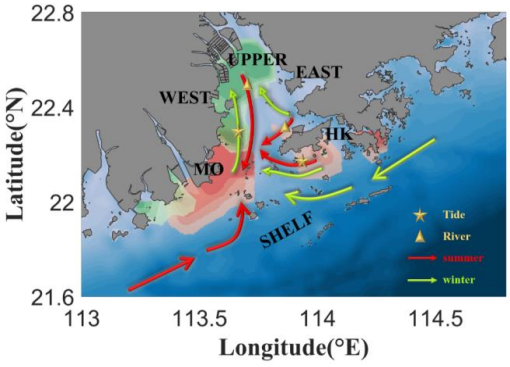

310 **Figure 9: The accumulation connections schematic in the PRE during summer (red arrow) and winter time (green arrow). The map color in red represented the high accumulation probabilities in summer, while in green represented winter. The star indicated tide dominated the current and triangle represented river discharge.**

https://doi.org/10.5194/egusphere-2024-106
Preprint. Discussion started: 31 January 2024

Data availability

All raw data can be provided by the corresponding authors upon request.

Author contributions

M.L conducted the investigation, methodology, and writing – original draft preparation; S.A conducted methodology and writing – review & editing; Z.C conducted the conceptualization, supervision, and writing – review & editing; T.Z. conducted the conceptualization and writing – review & editing.

Competing interests

The authors declare that they have no conflict of interest.

Acknowledgements

This work is supported by CORE which is a joint research centre for ocean research between Laoshan Laboratory and HKUST. The simulation was performed at the SICC, which is supported by the SKL-IOTSC, University of Macau.

Financial support

This work was funded by the Science and Technology Development Fund, Macau SAR (0093/2020/A2, 001/2024/SKL), The Open Research Project Programme of the State Key Laboratory of Internet of Things for Smart City (University of Macau) (Ref. No.: SKL-IoTSC(UM)-2021-2023/ORPF/A20/2022), National Natural Science Foundation of China (NSFC) under Project (42076026), Independent Research Project Program of State Key Laboratory of Tropical Oceanography (LTOZZ2102), General Research Fund (project ID 15216422) from the Research Grants Council of Hong Kong.

References

Acha, E. M., Mianzan, H. W., Guerrero, R. A., Favero, M., & Bava, J. (2004). Marine fronts at the continental shelves of austral South America: Physical and ecological processes. *Journal of marine systems, 44*(1), 83-105. doi:10.1016/j.jmarsys.2003.09.005

Ascione Kenov, I., Garcia, A. C., & Neves, R. (2012). Residence time of water in the Mondego estuary (Portugal). *Estuarine, coastal and shelf science, 106*, 13-22. doi:10.1016/j.ecss.2012.04.008

Banas, N. S., & Hickey, B. M. (2005). Mapping exchange and residence time in a model of Willapa Bay, Washington, a branching, macrotidal estuary. *Journal of Geophysical Research, 110*(C11), C11011-n/a. doi:10.1029/2005JC002950

https://doi.org/10.5194/egusphere-2024-106
Preprint. Discussion started: 31 January 2024

Cai, Z., Liu, G., Liu, Z., & Gan, J. (2022). Spatiotemporal variability of water exchanges in the Pearl River Estuary by interactive multiscale currents. *Estuarine, coastal and shelf science, 265*, 107730. doi:10.1016/j.ecss.2021.107730

Chenillat, F., Blanke, B., Grima, N., Franks, P. J. S., Capet, X., & Rivière, P. (2015). Quantifying tracer dynamics in moving fluids: a combined Eulerian-Lagrangian approach. *3*. doi:10.3389/fenvs.2015.00043

Chu, N., Liu, G., Xu, J., Yao, P., Du, Y., Liu, Z., & Cai, Z. (2022). Hydrodynamical transport structure and lagrangian connectivity of circulations in the Pearl River Estuary. *9*. doi:10.3389/fmars.2022.996551

Cui, L., Cai, Z., & Liu, Z. (2023). Water exchange and transport pathways in estuary-shelf region of Pearl River Estuary under multiple forcings. *Continental shelf research, 266*, 105099. doi:10.1016/j.csr.2023.105099

Dai, M., Guo, X., Zhai, W., Yuan, L., Wang, B., Wang, L., . . . Cai, W.-J. (2006). Oxygen depletion in the upper reach of the Pearl River estuary during a winter drought. *Marine chemistry, 102*(1), 159-169. doi:10.1016/j.marchem.2005.09.020

Dawson, M. N., Sen Gupta, A., & England, M. H. (2005). Coupled Biophysical Global Ocean Model and Molecular Genetic Analyses Identify Multiple Introductions of Cryptogenic Species. *Proceedings of the National Academy of Sciences - PNAS, 102*(34), 11968-11973. doi:10.1073/pnas.0503811102

Defontaine, S., Sous, D., Tesan, J., Monperrus, M., Lenoble, V., & Lanceleur, L. (2020). Microplastics in a salt-wedge estuary: Vertical structure and tidal dynamics. *Marine pollution bulletin, 160*, 111688. doi:https://doi.org/10.1016/j.marpolbul.2020.111688

Dippner, W. J. H. S. M. (2009). Mathematical modeling of the transport of pollution in water. *2*, 204-246.

Dong, L., Su, J., Ah Wong, L., Cao, Z., & Chen, J.-C. (2004). Seasonal variation and dynamics of the Pearl River plume. *Continental shelf research, 24*(16), 1761-1777. doi:10.1016/j.csr.2004.06.006

Drouin, K. L., & Lozier, M. S. (2019). The Surface Pathways of the South Atlantic: Revisiting the Cold and Warm Water Routes Using Observational Data. *Journal of geophysical research. Oceans, 124*(10), 7082-7103. doi:10.1029/2019JC015267

Drouin, K. L., Lozier, M. S., Beron-Vera, F. J., Miron, P., & Olascoaga, M. J. (2022). Surface Pathways Connecting the South and North Atlantic Oceans. *Geophysical research letters, 49*(1), n/a. doi:10.1029/2021GL096646

Fok, L., & Cheung, P. K. (2015). Hong Kong at the Pearl River Estuary: A hotspot of microplastic pollution. *Marine pollution bulletin, 99*(1), 112-118. doi:https://doi.org/10.1016/j.marpolbul.2015.07.050

Gong, W., Shen, J., & Hong, B. (2009). The influence of wind on the water age in the tidal Rappahannock River. *Marine Environmental Research, 68*(4), 203-216. doi:https://doi.org/10.1016/j.marenvres.2009.06.008

Guo, W., Ye, F., & Lian, Z. (2016). Seasonal changes of organic carbon in the Pearl River estuary. *Re dai hai yang xue bao, 35*(4), 40-50.

Haza, A. C., Özgökmen, T. M., & Hogan, P. (2016). Impact of submesoscales on surface material distribution in a gulf of Mexico mesoscale eddy. *Ocean modelling (Oxford), 107*, 28-47. doi:10.1016/j.ocemod.2016.10.002

He, C., Yin, Z.-Y., Stocchino, A., & Wai, O. W. H. (2023). Generation of macro-vortices in estuarine compound channels. *Frontiers in Marine Science, 10*. doi:10.3389/fmars.2023.1082506

He, C., Yin, Z.-Y., Stocchino, A., Wai, O. W. H., & Li, S. (2022). The coastal macro-vortices dynamics in Hong Kong waters and its impact on water quality. *Ocean Modelling, 175*, 102034. doi:https://doi.org/10.1016/j.ocemod.2022.102034

He, Q., Zhan, H., Cai, S., He, Y., Huang, G., & Zhan, W. (2018). A New Assessment of Mesoscale Eddies in the South China Sea: Surface Features, Three-Dimensional Structures, and Thermohaline Transports. *123*(7), 4906-4929. doi:https://doi.org/10.1029/2018JC014054

Hinojosa, I. A., Rivadeneira, M. M., & Thiel, M. (2011). Temporal and spatial distribution of floating objects in coastal waters of central–southern Chile and Patagonian fjords. *Continental shelf research, 31*(3), 172-186. doi:10.1016/j.csr.2010.04.013

https://doi.org/10.5194/egusphere-2024-106
Preprint. Discussion started: 31 January 2024

Jalón-Rojas, I., Wang, X. H., & Fredj, E. (2019). Technical note: On the importance of a three-dimensional approach for modelling the transport of neustic microplastics. *Ocean Sci., 15*(3), 717-724. doi:10.5194/os-15-717-2019

Jönsson, B. F., & Watson, J. R. (2016). The timescales of global surface-ocean connectivity. *Nature communications, 7*(1), 11239-11239. doi:10.1038/ncomms11239

Lebreton, L. C. M., Greer, S. D., & Borrero, J. C. (2012). Numerical modelling of floating debris in the world's oceans. *Marine pollution bulletin, 64*(3), 653-661. doi:https://doi.org/10.1016/j.marpolbul.2011.10.027

Li, D., Gan, J., Hui, C., Yu, L., Liu, Z., Lu, Z., . . . Dai, M. (2021). Spatiotemporal Development and Dissipation of Hypoxia Induced by Variable Wind-Driven Shelf Circulation off the Pearl River Estuary: Observational and Modeling Studies. *126*(2), e2020JC016700. doi:https://doi.org/10.1029/2020JC016700

Li, X., Lu, C., Zhang, Y., Zhao, H., Wang, J., Liu, H., & Yin, K. (2020). Low dissolved oxygen in the Pearl River estuary in summer: Long-term spatio-temporal patterns, trends, and regulating factors. *Marine pollution bulletin, 151*, 110814-110814. doi:10.1016/j.marpolbul.2019.110814

Liang, J.-H., Liu, J., Benfield, M., Justic, D., Holstein, D., Liu, B., . . . Dong, W. (2021). Including the effects of subsurface currents on buoyant particles in Lagrangian particle tracking models: Model development and its application to the study of riverborne plastics over the Louisiana/Texas shelf. *Ocean modelling (Oxford), 167*, 101879. doi:10.1016/j.ocemod.2021.101879

Lima, A. R. A., Barletta, M., & Costa, M. F. (2015). Seasonal distribution and interactions between plankton and microplastics in a tropical estuary. *Estuarine Coastal and Shelf Science, 165*, 213-225. doi:10.1016/j.ecss.2015.05.018

Lima, A. R. A., Costa, M. F., & Barletta, M. (2014). Distribution patterns of microplastics within the plankton of a tropical estuary. *Environmental research, 132*, 146-155. doi:10.1016/j.envres.2014.03.031

Liu, Z., Zu, T., & Gan, J. (2020). Dynamics of cross-shelf water exchanges off Pearl River Estuary in summer. *Progress in Oceanography, 189*, 102465. doi:https://doi.org/10.1016/j.pocean.2020.102465

Malli, A., Corella-Puertas, E., Hajjar, C., & Boulay, A.-M. (2022). Transport mechanisms and fate of microplastics in estuarine compartments: A review. *Marine pollution bulletin, 177*, 113553-113553. doi:10.1016/j.marpolbul.2022.113553

Mao, Q., Shi, P., Yin, K., Gan, J., & Qi, Y. (2004). Tides and tidal currents in the Pearl River Estuary. *Continental shelf research, 24*(16), 1797-1808. doi:10.1016/j.csr.2004.06.008

Miron, P., Beron-Vera, F. J., Helfmann, L., & Koltai, P. (2021). Transition paths of marine debris and the stability of the garbage patches. *Chaos (Woodbury, N.Y.), 31*(3), 033101-033101. doi:10.1063/5.0030535

Miron, P., Beron-Vera, F. J., Olascoaga, M. J., Froyland, G., Pérez-Brunius, P., & Sheinbaum, J. (2019). Lagrangian Geography of the Deep Gulf of Mexico. *Journal of physical oceanography, 49*(1), 269-290. doi:10.1175/JPO-D-18-0073.1

Miron, P., Beron-Vera, F. J., Olascoaga, M. J., Sheinbaum, J., Pérez-Brunius, P., & Froyland, G. (2017). Lagrangian dynamical geography of the Gulf of Mexico. *Scientific reports, 7*(1), 7021-7021. doi:10.1038/s41598-017-07177-w

North, E. W., Adams, E. E. E., Schlag, Z. Z., Sherwood, C. R., He, R. R., Hyun, K. H. K., . . . Enterprise, M. t. D. H. O. S. A. R. B. (2011). Simulating oil droplet dispersal from the Deepwater Horizon spill with a Lagrangian approach. *195*, 217-226.

North, E. W., Hood, R. R., Chao, S. Y., & Sanford, L. P. (2006). Using a random displacement model to simulate turbulent particle motion in a baroclinic frontal zone: A new implementation scheme and model performance tests. *Journal of marine systems, 60*(3), 365-380. doi:10.1016/j.jmarsys.2005.08.003

Paris, C. B., Hénaff, M. L., Aman, Z. M., Subramaniam, A., Helgers, J., Wang, D.-P., . . . Srinivasan, A. (2012). Evolution of the Macondo Well Blowout: Simulating the Effects of the Circulation and Synthetic Dispersants on the Subsea

https://doi.org/10.5194/egusphere-2024-106
Preprint. Discussion started: 31 January 2024

Oil Transport. *Environmental Science & Technology, 46*(24), 13293-13302. doi:10.1021/es303197h

Shchepetkin, A. F., & McWilliams, J. C. (2005). The regional oceanic modeling system (ROMS): a split-explicit, free-surface, topography-following-coordinate oceanic model. *Ocean modelling (Oxford), 9*(4), 347-404. doi:10.1016/j.ocemod.2004.08.002

Song, Y., & Haidvogel, D. (1994). A Semi-implicit Ocean Circulation Model Using a Generalized Topography-Following Coordinate System. *Journal of Computational Physics, 115*(1), 228-244. doi:https://doi.org/10.1006/jcph.1994.1189

van Sebille, E., Griffies, S. M., Abernathey, R., Adams, T. P., Berloff, P., Biastoch, A., . . . Zika, J. D. (2018). Lagrangian ocean analysis: Fundamentals and practices. *Ocean modelling (Oxford), 121*(C), 49-75. doi:10.1016/j.ocemod.2017.11.008

Vermeiren, P., Muñoz, C. C., & Ikejima, K. (2016). Sources and sinks of plastic debris in estuaries: A conceptual model integrating biological, physical and chemical distribution mechanisms. *Marine pollution bulletin, 113*(1-2), 7-16. doi:10.1016/j.marpolbul.2016.10.002

Wang, T., Zhao, S., Zhu, L., McWilliams, J. C., Galgani, L., Amin, R. M., . . . Chen, M. (2022). Accumulation, transformation and transport of microplastics in estuarine fronts. *Nature Reviews Earth & Environment, 3*(11), 795-805. doi:10.1038/s43017-022-00349-x

Zhong, L., & Li, M. (2006). Tidal energy fluxes and dissipation in the Chesapeake Bay. *Continental shelf research, 26*(6), 752-770. doi:https://doi.org/10.1016/j.csr.2006.02.006

Zu, T., & Gan, J. (2015). A numerical study of coupled estuary–shelf circulation around the Pearl River Estuary during summer: Responses to variable winds, tides and river discharge. *Deep Sea Research Part II: Topical Studies in Oceanography, 117*, 53-64. doi:https://doi.org/10.1016/j.dsr2.2013.12.010

Zu, T., Gan, J., & Erofeeva, S. Y. (2008). Numerical study of the tide and tidal dynamics in the South China Sea. *Deep Sea Research Part I: Oceanographic Research Papers, 55*(2), 137-154. doi:https://doi.org/10.1016/j.dsr.2007.10.007